# THE SPIRE INSTRUMENT FOR HERSCHEL

**M.J. Griffin[1], B.M. Swinyard[2], and L. Vigroux[3]**

[1]Physics Dept., Queen Mary, University of London, UK
[2]Rutherford Appleton Laboratory, Oxfordshire, UK
[3]CEA Service d'Astrophysique, Saclay, France

## Abstract

SPIRE, the Spectral and Photometric Imaging Receiver, will be a bolometer instrument for ESA's Herschel satellite. Its main scientific goals are deep extragalactic and galactic imaging surveys and spectroscopy of star-forming regions in own and nearby galaxies. The SPIRE detectors are feedhorn-coupled NTD "spider-web" bolometers. The instrument comprises a three-band imaging photometer covering the 250-500 $\mu$m range, and an imaging Fourier Transform Spectrometer (FTS) covering 200-670 $\mu$m. The photometer has a field of view of 4 x 8 arcminutes which is observed simultaneously at 250, 350 and 500 $\mu$m, with dichroic beam dividers separating the three spectral bands. Its angular resolution is determined by the telescope diffraction limit, with FWHM beam widths of approximately 17, 24 and 35 arcseconds at 250, 350 and 500 $\mu$m, respectively. An internal beam steering mirror can be used for spatial modulation of the telescope beam, and observations can also be made by scanning the telescope without chopping, providing better sensitivity for source confusion-limited deep surveys. The FTS has a field of view of 2.6 arcminutes and an adjustable spectral resolution of 0.04 - 2 cm$^{-1}$ ($\lambda/\Delta\lambda$ = 20 - 1000 at 250 $\mu$m). It employs a dual-beam configuration with novel broad-band intensity beam dividers to provide high efficiency and separated output and input ports.

Key words: Herschel–Submillimetre–Instrumentation

## 1. Introduction

SPIRE (the Spectral and Photometric Imaging REceiver) is one of three cryogenic focal plane instruments for ESA's Herschel mission. Its main scientific goals are the investigation of the statistics and physics of galaxy and structure formation at high redshift and the study of the earliest stages of star formation, when the protostar is still coupled to the interstellar medium. These studies require the capabilities to carry out large-area (many tens of square degrees) deep photometric imaging surveys at far-infrared and submillimetre wavelengths, and to follow up these systematic survey observations with spectroscopy of selected sources. SPIRE will exploit the advantages of Herschel: its large-aperture, cold, low-emissivity telescope; the complete lack of atmospheric emission and attenuation giving access to the poorly explored 200-700-$\mu$m range; and the large amount of high quality observing time. Because of these advantages, SPIRE will have unmatched sensitivity for deep imaging photometry and moderate-resolution spectroscopy.

Galaxies emit a large proportion (from 30% to nearly 100%) of their total energy output in the far infrared due to re-processing of stellar UV radiation by interstellar dust grains. The far infrared peak is redshifted into the SPIRE wavelength range for galaxies with redshift beyond $\sim$ 1. The total luminosity of a galaxy cannot be determined without an accurate measurement of its Spectral Energy Distribution (SED). The study of the early stages of galaxy evolution thus requires an instrument that can detect emission from high-z galaxies in the submillimetre, enabling their SEDs and luminosities to be derived. The pioneering observations made with the SCUBA submillimetre camera on the JCMT have emphasised the importance of the FIR-submillimetre band for studies of the high-redshift universe (e.g., Hughes et al. 1998, Smail et al. 1999, Eales et al. 2000).

Stars form through the fragmentation and collapse of dense cloud cores in the interstellar medium (ISM), and the very first stages of this process are not well understood. A good understanding of this early evolution is crucial, as it governs the origin of the stellar initial mass function (IMF). Sensitive far infrared and submillimetre observations with high spatial resolution are necessary to make complete surveys of protostellar clumps to determine their bolometric luminosities and mass functions. SPIRE will also, for the first time, enable astronomers to observe at high spatial resolution the physical and chemical conditions prevailing in the cold phases of the interstellar medium and to study the behavior of the interstellar gas and dust before and during star formation. SPIRE's uniquely high sensitivity to very cold dust emission also makes it the ideal instrument to study the material that is ejected in copious quantities from evolved stars, enriching the interstellar medium with heavy elements. Large amounts of matter - as yet undetected - are ejected from stars before the white dwarf stage. Theories of stellar evolution, and of the enrichment of galaxies in heavy elements and dust, will be incomplete until these earlier mass loss

Proc. of *'The Promise of FIRST'* symposium, 12–15 December 2000, Toledo, Spain (G.L. Pilbratt, J. Cernicharo, A.M. Heras, T. Prusti, & R. Harris eds., ESA SP-460, Month, 2001)

phases are characterised and understood. Studies of star formation and of the interaction of forming and evolved stars with the ISM are also, of course, intimately related to the investigation of galaxy formation and evolution, which occur through just these processes.

These high priority programmes for Herschel require sensitive continuum imaging in several bands to carry out surveys, and a low-resolution spectroscopic mode to obtain detailed SEDs of selected objects and measure key spectral lines. Although SPIRE has been optimised for these two main scientific programmes, it will offer the astronomical community a powerful tool for many other astrophysical studies: giant planets, comets, the galactic interstellar medium, nearby galaxies, ultraluminous infrared galaxies, and active galactic nuclei.

## 2. Instrument overview

SPIRE contains a three-band imaging photometer and an imaging Fourier Transform Spectrometer (FTS), both of which use 0.3-K feedhorn-coupled "spider-web" NTD germanium bolometers cooled by a $^3$He refrigerator. The photometer and spectrometer are not designed to operate simultaneously. The field of view of the photometer is 4 x 8 arcminutes, the largest that can be achieved given the location of the SPIRE field of view in the Herschel focal plane and the size of the telescope unvignetted field of view. Three bolometer arrays provide broad-band photometry ($\lambda/\Delta\lambda \simeq 3$) in wavelength bands centred on 250, 350 and 500 $\mu$m. The field of view is observed simultaneously in all three bands through the use of fixed dichroic beam-splitters. Spatial modulation can be provided either by a Beam Steering Mirror (BSM) in the instrument or by drift scanning the telescope across the sky, depending on the type of observation. An internal thermal calibration source is available to provide a repeatable calibration signal for the detectors. The FTS uses novel broad-band intensity beam dividers, and combines high efficiency with spatially separated input ports. One input port covers a 2.6-arcminute diameter field of view on the sky and the other is fed by an on-board calibration source. Two bolometer arrays are located at the output ports, one covering 200-300 $\mu$m and the other 300-670 $\mu$m. The FTS will be operated in continuous scan mode, with the path difference between the two arms of the interferometer being varied by a constant-speed mirror drive mechanism. The spectral resolution, as determined by the maximum optical path difference, will be adjustable between 0.04 and 2 cm$^{-1}$ (corresponding to $\lambda/\Delta\lambda$ = 1000 - 20 at 250 $\mu$m wavelength).

The focal plane unit is approximately 690 x 410 x 410 mm in size, and has three separate temperature stages at nominal temperatures of 4 K, 2 K (provided by the Herschel cryostat) and 300 mK (provided by SPIRE's internal cooler). The main 4-K structural element of the FPU is an optical bench panel which is supported from the 10-K cryostat optical bench by stainless steel blade mounts. The photometer and spectrometer are located on either side of this panel. The majority of the optics are at 4 K, but the detector arrays and final optics are contained within 2-K enclosures. The $^3$He refrigerator cools all of the five detector arrays to 0.3 K. Two JFET preamplifier boxes (one for the photometer and one for the FTS) are attached to the 10-K optical bench close to the 4-K enclosure, with the JFETs heated internally to their optimum operating temperature of $\sim$ 120 K.

The SPIRE warm electronics consist of a Detector Readout and Control Unit (DRCU) and a Digital Processing Unit (DPU). The DRCU provides bias and signal conditioning for the arrays and cold readout electronics, reads out the detector signals, and controls the FPU mechanisms and the $^3$He cooler. The DPU acts as the interface to the spacecraft, including instrument commanding, and formats science and housekeeping data for telemetry to the ground.

## 3. Imaging photometer

### 3.1. Optical design and FPU layout

The photometer layout is shown in Fig. 1. The 4-K optical elements are mounted directly from the optical bench panel. The 2-K enclosure is also supported from the panel by stainless steel blades, and contains the detector arrays, dichroics, and fold mirrors. The three array modules are bolted to the outside wall of the 2-K box. Within each module, the detector arrays, feedhorns and the final filter are thermally isolated from the 2-K structure by Kevlar wires, and are cooled by a thermal strap to the $^3$He refrigerator (see section 5 below). The photometer input optics are shared with the spectrometer. The separate spectrometer field of view is directed to the other side of the optical bench panel by a pick-off mirror.

The optical design of the photometer is shown in Fig. 2, and is described in more detail by Dohlen et al. (2000) It is an all-reflective system except for two dichroic beam dividers used to direct the three wavelength bands onto different bolometer arrays, and various transmissive band-pass and edge filters used to reject out-of-band radiation. It is optimised to give close to diffraction-limited imaging across the whole 4 x 8 arcminute field of view. The SPIRE field of view is offset by 11 arcminutes from the centre of the Herschel telescope's highly curved focal surface. Mirror M3, which lies below the focus, receives the f/8.68 beam from the telescope and forms a pupil image of the telescope secondary at the flat beam steering mirror, M4. Mirror M5 converts the focal ratio to f/5 and provides an intermediate focus at the next mirror, M6, which re-images the aperture stop at M4 to a cold stop located at the entrance to a 2-K enclosure. M7, M8 and M9 constitute a one-to-one optical relay to bring the M6 focus to the three detector arrays. The beams for the three bands are directed onto the arrays at f/5 by a combination of

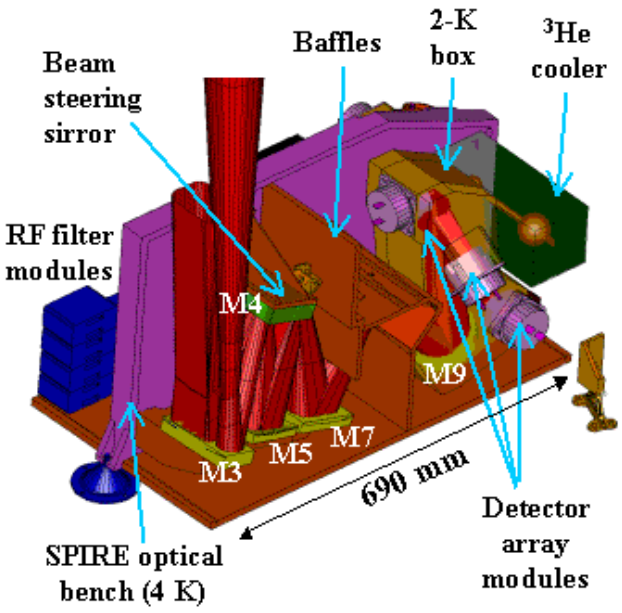


*Figure 1.* Photometer FPU layout

flat folding mirrors and fixed dichroics set at 25$^o$ to the beam axis. M3 - M8 are at 4 K and the cold stop and all subsequent optics are at 2 K.

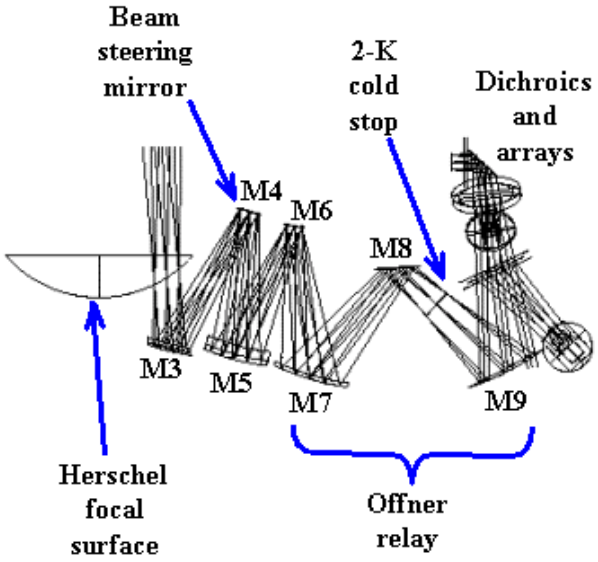


*Figure 2.* Photometer optical design

A shutter at the entrance aperture of the instrument (just above the telescope focus) can be inserted to block the beam. This will be important for ground testing in the Herschel cryostat where the background radiation from the cryostat shields and lid will be much greater than in flight. The shutter will allow the detector performance to be tested and verified under controlled flight-representative conditions. Flight operation of the shutter is not planned.

An internal calibration source provides a repeatable signal for the bolometer arrays. It radiates through a 1-mm hole in the centre of the beam steering mirror, M4. As this is at a pupil image, the illumination is close to uniform over the arrays. The source can be modulated at frequencies up to 5 Hz, and operated at temperatures up to 80 K to give sufficient signal on the arrays, with peak power dissipation $\leq$ 2 mW. The beam steering mirror is capable of chopping $\pm$ 2 arcminutes along the long axis of the 4 x 8 arcminute field of view, at frequencies up to 2 Hz with an efficiency of 90% and power dissipation $\leq$ 2 mW. It can operate at higher frequencies with reduced efficiency and increased power dissipation. The beam steering mechanism can simultaneously chop at up to 1 Hz in the orthogonal direction by up to 30 arcseconds. Two axis motion allows "jiggling" of the pointing to create a fully sampled image of the sky with the feedhorn-coupled detectors whose diffraction-limited beams on the sky are separated by approximately twice the beam FWHM.

The SPIRE filtering scheme is designed to provide precise definition of the spectral passbands with high out-of-band rejection and maximum in-band transmission, and also to minimise the thermal loading on the 4-K, 2-K and 0.3-K stages by reflecting short-wavelength radiation. To achieve complete rejection out to UV wavelengths, four blocking filters are needed in the chain in addition to high-pass and low-pass edge filters which define the band. Figure 3 shows the measured transmission profiles for a prototype 350-$\mu$m band filter set.

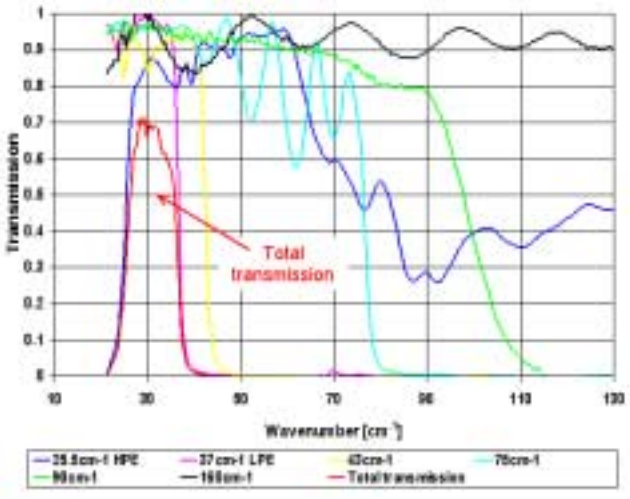


*Figure 3.* SPIRE 350-$\mu$m band prototype filtering scheme

### 3.2. Detector arrays

SPIRE will use spider-web bolometers with NTD germanium thermometers (Mauskopf et al. 1997, Bock et al. 1998). The bolometers are coupled to the telescope by hexagonally close-packed $2F\lambda$ diameter single-mode conical feedhorns, providing diffraction limited beams. Modelling of the complete optical train predicts FWHM beam widths of 17.1, 24.4 and 34.6 arcseconds at 250, 350 and 500 $\mu$m respectively. The numbers of detectors in the three arrays are 139, 88, and 43 for 250, 350 and 500 $\mu$m respectively, making a total of 270 detectors for the photometer. The detector arrays are shown schematically in Fig. 4a, and a photograph of a prototype array module is shown in Fig. 4b. Each array unit has an interface to the 2-K box, with a thermal strap from the $^3$He cooler to the 0.3-K stage, which is supported by Kevlar strings from the 2-K level. The electrical connections to the detectors are made with Kapton ribbon cables within the array modules and with woven manganin cables between the array modules and the JFET units. The bolometers are excited by an AC bias at approx. 100 Hz, which eliminates 1/f noise from the JFETs, giving a 1/f knee for the system of less than 100 mHz. Conservative estimates of the bolometer Detective Quantum Efficiency (DQE) vary between 0.6 and 0.7 ensuring that the overall NEP will be dominated by the thermal emission from the Herschel telescope.

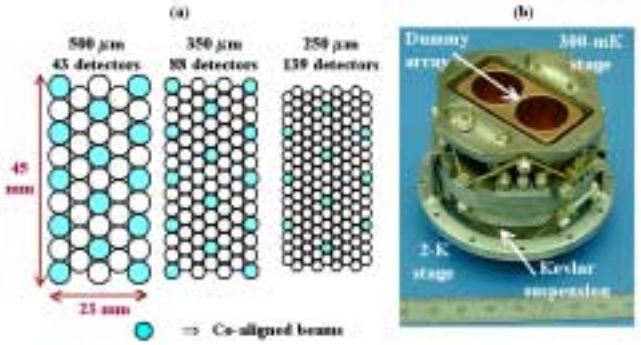


*Figure 4. Photometer arrays and bolometer array unit mechanical prototype*

### 3.3. Photometer observing modes

The photometer will have three principal observing modes, as illustrated in Fig. 5 and described below.

Point source photometry: For photometric observations of point or compact sources, chopping will be used. There are several sets of three detectors for which the beams at the three wavelengths are exactly co-aligned on the sky, indicated by the shaded circles in Fig. 5. By chopping through the appropriate angle (approx. 126 arcseconds), 3-band photometric observations can be carried out simultaneously with maximum efficiency. To account for

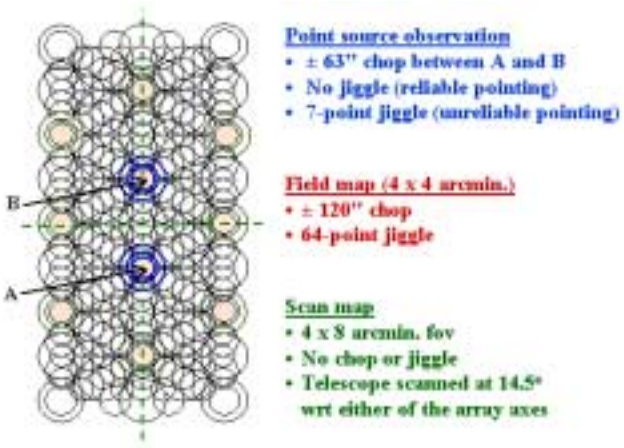


*Figure 5.* Photometer observing modes

the possibility of positional errors due to telescope pointing inaccuracy or imperfect knowledge of the source position, the beam steering mirror can be used to implement a seven-point mapping routine in this mode. Assuming an angular offset of 6" for the seven-point, the loss in S/N for a given integration time varies between 6% at 500 $\mu$m and 20% at 250 $\mu$m, which is a small penalty to pay for assurance that telescope pointing or source position errors do not result in an underestimate of the source flux density.

Field mapping: For mapping of regions a few arcminutes in extent, the beam steering mirror will be used to carry out a jiggle map, similar to the mode of operation of the SCUBA bolometer camera on the JCMT (Holland et al. 1999). A 64-point jiggle pattern is needed to achieve full spatial sampling in all bands simultaneously, with a step size of 9 arcseconds (half-beam spacing at 250 $\mu$m). A maximum field size of 4 x 4 arcminutes is available in this mode as the 2-arcminute regions at each end of the array will be chopped outside the field of view admitted by the photometer optics.

Scan mapping: This mode will be used for mapping large areas of sky (much bigger than the SPIRE field of view), including deep survey observations. The telescope will be scanned across the sky (at up to 1 arcminute per second, the maximum rate that the spacecraft can provide). Because of the excellent 1/f stability of the NTD detectors, the beam steering mirror does not need to be operated - signal modulation is provided by the telescope motion. To provide the necessary beam overlap for full spatial sampling over the strip defined by a single scan, the scan angle must be $14.5^o$ with respect to one of the array axes.

The available telemetry rate of 100 kbs allows all of the 270 photometer detectors to be sampled with 16-bit resolution at up to 28 Hz and the data telemetered directly to the ground with no on-board processing (we assume an observing efficiency of 0.9).

## 4. Fourier transform spectrometer

### 4.1. Optical design and FPU layout

The layout of the FTS and its optical scheme are shown in Figs. 6 and 7 respectively. The FTS (Swinyard et al. 2000) uses two broadband, high-efficiency, intensity beam splitters in a Mach-Zehnder configuration rather than the traditional polarising beam dividers. This configuration has the advantage that all four ports are separately accessible, as in the classical Martin Puplett (M-P) polarising FTS. But the throughput is a factor of two higher than for the M-P as none of the incoming radiation is rejected. This design is also insensitive to the polarisation of the incident radiation. The performance of the beam dividers and of a bench-top implementation of this design has been demonstrated (Ade et al. 1999). A thermal calibrator is located at a pupil image in the second input port of the FTS, and provides a thermal input that mimics the dilute 80-K black body emission of the telescope. This allows the large telescope background to be nulled, thereby reducing the dynamic range requirements for the detector sampling. Two band-limited detector arrays are placed in the two output ports, covering 200-300 $\mu$m and 300-670 $\mu$m. A single back-to-back moving roof-top mechanism serves both arms of the interferometer, with a frictionless carriage mechanism using double parallelogram linkage and flex pivots. The pick-off mirror (on the photometer side of the optical bench panel and located at the intermediate field image) directs the spectrometer field of view through a hole in the optical bench panel into the FTS side of the instrument. A 4-K pupil stop is located between the pick-off mirror and the input fold mirror. The input relay mirror focuses the beam to an intermediate image plane located just after the first beam divider, after which the beam is collimated and sent to the moving corner cube assembly. The corner cube shifts the beam and sends it towards the camera mirror, which produces an image plane just before the output beam divider. The output relay mirror focuses the beam onto the detector arrays. A pupil image is located near the final fold mirror, making this a convenient location for the entrance aperture to the 2-K enclosure. As this pupil moves when the optical path difference changes, it is not a good place for a limiting cold stop. Instead, the limiting aperture is located at the 4-K pupil plane between the pick-off mirror and the input fold mirror.

The FTS design is optimised for the 200-400 $\mu$m band. The wavelength coverage is extended to 15 cm$^{-1}$ (670 $\mu$m) to give access to the astrophysically important 609-$\mu$m line of CI in our own and nearby galaxies, and to increase the range over which the spectral energy distribution of sources can be measured in the FTS low-resolution mode. A filtering scheme similar to the one employed for the photometer channel is used to restrict the passband of the instrument. Filters on the bolometer arrays themselves define the passband for each array.

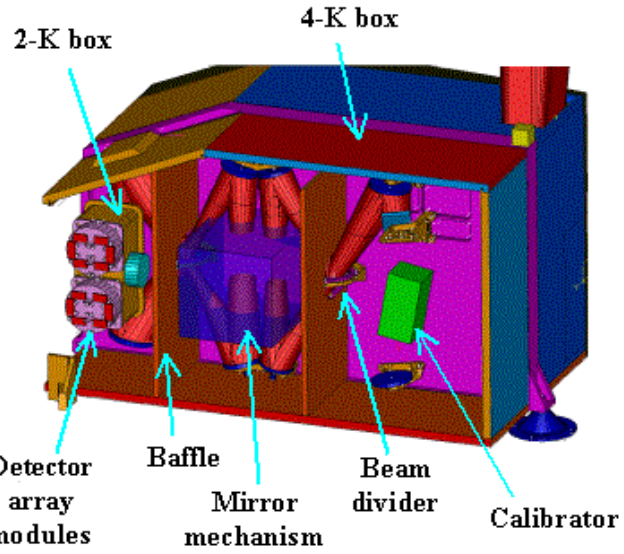


*Figure 6.* Spectrometer FPU layout

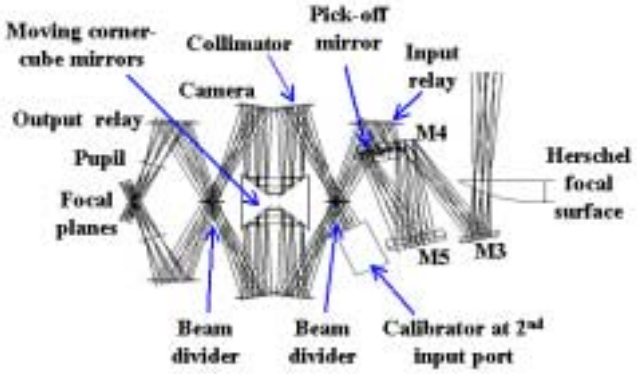


*Figure 7.* Spectrometer optical design

### 4.2. Spectrometer arrays

The field of view of the FTS is approximately 2.6 arcminutes in diameter, and is covered by 37 hexagonally close-packed detectors in a short-wavelength array and 19 in a long-wavelength array. The detector modules will be similar to those used for the photometer, with a mechanical interface to the wall of the 2-K enclosure.

The two FTS arrays cover the 200-300 and 300-670 $\mu$m bands. The detectors and feedhorns for the short wavelength band are similar to those for the photometer 250 $\mu$m channel. The long wavelength band is optimised for the 300-400 $\mu$m range. There is a degradation in point source coupling efficiency at wavelengths beyond around 400 $\mu$m due to the decreasing aperture size relative to the wavelength. The waveguide coupling the horn to the bolometer must also have a diameter large enough to transmit at 670 $\mu$m, and so is overmoded at the shorter wavelengths within the band. This results in an increase in background radiation on the detectors and a broadening

of the beam by about 20% compared to the diffraction limit at the lower end of the band (Caldwell et al. 2000).

The layout of the FTS arrays is shown in Fig. 8. The detectors on the periphery of the arrays are partly vignetted by the 2.6-arcminute field of view admitted by the instrument optics (indicated by the large circles in Fig. 8). The short-wavelength array feedhorns are sized to give 2F$\lambda$ pixels at 225 $\mu$m and the long-wavelength horns to give 2F$\lambda$ pixels at 389 $\mu$m. This arrangement, although slightly non-optimal from the point of view of point source sensitivity at the central wavelengths of the two arrays, has the advantage that there are numerous co-aligned pixels in the combined field of view. This maximises the observing efficiency for measuring a point source spectrum together with its surrounding sky background and also provides redundancy to the spectrometer in the case of failure of a single pixel within one array.

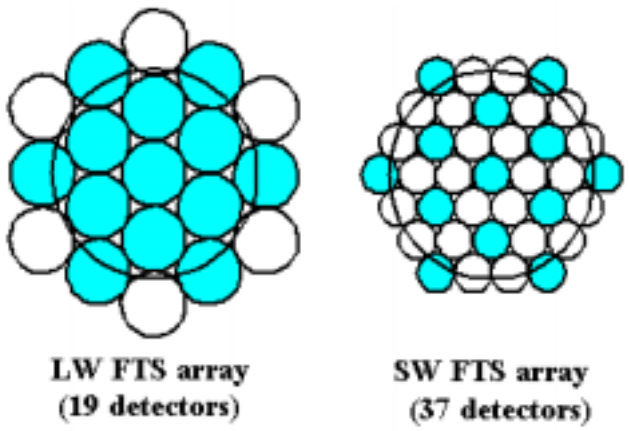


*Figure 8. Spectrometer detector arrays. The shaded detecors are co-aligned on the sky in the two bands.*

### 4.3. Spectrometer observing modes

The FTS will be operated in continuous scan mode with the mirrors moving at a constant speed of up to 0.1 cm $s^{-1}$, corresponding to a signal frequency range of 6 - 20 Hz. The spectral resolution can be adjusted between 0.04 and 2 $cm^{-1}$ ($\lambda/\Delta\lambda$ = 20 - 1000 at 250 $\mu$m). The maximum scan length is 3.5 cm (taking 35 seconds or more and giving an optical path difference of 14 cm). To ensure that mechanism jitter noise is well below the photon noise level, a relative accuracy of 0.1 $\mu$m is required for the mirror position. The FTS calibration source will be on continuously while the spectrometer is operating, with a peak power of no more than 5 mW. For spectral mapping of extended sources, the beam steering mirror will be used to provide the necessary pointing changes between scans. The scanning mirror control system uses a digital feedback loop to provide a constant speed over the scan length, with an accuracy requirement of 1% (goal 0.5%). The position readout uses a Heidenhain (http://www.heidenhain.de) Moiré fringe sensing system. The detectors are read out asynchronously with the samples time-stamped to match them to the corresponding mirror locations. No on-board processing will be done - the raw interferograms will be telemetered to the ground. The number of detectors and the available telemetry rate are compatible with an oversampling factor of 2 with respect to the Nyquist sampling rate of 40 Hz (sampling at approx. 80 Hz per detector). An oversampling factor somewhat greater than this is desirable - options to achieve this include increasing the data rate, decreasing the mirror speed, sampling only a fraction of the detectors in some cases (e.g., point source observations), or a combination of these.

## 5. $^3$He cooler

The $^3$He cooler (Duband 1997) uses porous material to adsorb or release a gas when cooled or heated. This type of refrigerator is well-suited to a space environment. Gas gap heat switches are used the control the refrigerator and there are no moving parts. It can be recycled indefinitely with over 95% duty cycle efficiency and the lifetime is only limited by that of the cold stage from which it is run (in this case, the lifetime of the Herschel cryostat). The evaporation of $^3$He naturally provides a very stable operating temperature under constant heat load over the entire cycle. The cooler requires no mechanical or vacuum connections and only low-current electrical leads for its operation, making the mechanical and electrical interfaces very simple. For operation in a zero-g environment two aspects of the design of a $^3$He refrigerator have been addressed: the liquid confinement and the structural strength required for the launch. The confinement within the evaporator is provided by a porous material which holds the liquid by capillary attraction. For the thermal isolation and structural support of the refrigerator elements, a suspension system using Kevlar wires has been designed to support the cooler firmly during launch whilst minimising the parasitic heat load on the system. The base-line SPIRE cooler contains 6 STP litres of $^3$He, fits in a 200 x 100 x 100 mm envelope and weighs about 1.6 kg. Its performance has been analysed using the same methods that successfully predicted the performance of the IRTS cooler on orbit. When operated from a 1.8-K heat sink it achieves a temperature of 287 mK at the yevaporator with a 10 $\mu$W heat load, a hold time of at least 46 hours and a duty cycle efficiency of 96%. The energy input to the helium tank during recycling of the fridge is about 700 Joules. The $^3$He cooler is a potential single point failure for the instrument. Its reliability and redundancy are under analysis, and an option with double parallel heat switches is being considered.

## 6. Performance estimation

The sensitivity of SPIRE has been estimated under the assumptions listed below. Pessimistic overall optical efficiencies of 30% for the photometer and 15% for the FTS are assumed, taking into account all losses including filter transmission, mirror reflectivity, diffraction within the instrument and pupil alignment errors.

*Table 1. Assumptions for SPIRE performance estimation.*

| **Item** | **Assumption** |
|---|---|
| Telescope temperature (K) | 80 |
| Telescope used diameter (m) | 3.29 |
| Telescope emissivity | 0.04 |
| **Photometer** | |
| Throughput | $\lambda^2$ |
| Bands ($\mu$m) | 250, 350 and 500 |
| Numbers of detectors | 139, 88 and 43 |
| Beam FWHM (arcsec.) | 17.4, 24.4 and 34.6 |
| Bolometer DQE | 0.6, 0.7 and 0.7 |
| Feed-horn/cavity efficiency | 0.70 |
| Field of view (arcmin.) | 4 x 8 |
| Overall instrument transmission | 0.3 |
| Filter widths ($\lambda/\Delta\lambda$) | 3.3 |
| Observing efficiency | 0.9 |
| **FTS spectrometer** | |
| Nominal bands ($\mu$m) | 200-300 and 300-670 |
| Numbers of detectors | 37, 19 |
| Bolometer DQE | 0.65 |
| Feed-horn/cavity efficiency | 0.70 |
| Field of view (arcmin.) | 2.6 |
| Max. spectral resolution ($cm^{-1}$) | 0.04 |
| Overall instrument transmission | 0.15 |
| Signal modulation efficiency | 0.5 |
| Observing efficiency | 0.8 |
| Electrical filter efficiency | 0.8 |

The nominal background power levels on the detectors (which are dominated by the telescope thermal emission), and the corresponding photon noise limited NEP values are given in Table 2.

The instrument sensitivity levels for the photometer and FTS are summarised in Tables 3 and 4. The figures quoted are the nominal values, with an overall uncertainty of around 50% to take into account uncertainties in instrument parameters, particularly feedhorn efficiency, detector DQE, and overall transmission efficiency.

The extragalactic confusion limit for SPIRE is in the region of 10-20 mJy (depending on the wavelength, the adopted source count model, and how one chooses to define the confusion limit). The photometer is capable of integrating down to the Herschel confusion limit with a sensitivity of 5 $\sigma$ in a time of 15 minutes or less. This will allow large area confusion-limited deep surveys to be carried out at a rate on the order of 0.5 square degrees per day. The FTS will be used to follow up brighter sources from this survey (and other existing catalogues) to determine the SEDs and carry out spectral line surveys with simultaneous coverage of the 200 - 670 $\mu$m band.

*Table 2. Background power (pW) and photon noise-limited NEPs ($WHz^{-1/2} \times 10^{-17}$) for SPIRE*

| Photometer Band ($\mu$m) | 250 | 350 | 500 |
|---|---|---|---|
| Background power | 3.9 | 3.2 | 2.4 |
| $NEP_{ph}$ | 8.1 | 6.1 | 4.5 |
| FTS Band ($\mu$m) | 200-300 | 300-670 | |
| Background power | 6.0 | 11 | |
| $NEP_{ph}$ | 10 | 11 | |

*Table 3. SPIRE sensitivity: photometry – mJy 5 $\sigma$; 1 hr*

| Band ($\mu$m) | 250 | 350 | 500 |
|---|---|---|---|
| Point source | 2.3 | 2.3 | 2.4 |
| 4' x 4' jiggle map | 8.8 | 8.7 | 9.1 |
| 4' x 8' scan map | 7.3 | 7.2 | 7.5 |

*Table 4. SPIRE sensitivity: spectroscopy – 5 $\sigma$; 1 hr*

| Line spectroscopy ($\Delta\sigma = 0.04\ cm^{-1}$) | | | |
|---|---|---|---|
| Wavelength ($\mu$m) | 200 | 400 | 670 |
| Point source; ($Wm^{-2} \times 10^{-17}$) | 3.5 | 3.8 | 7.5 |
| Map; $\Delta$S ($Wm^{-2} \times 10^{-17}$) | 9.4 | 10 | 20 |
| Spectrophotometry ($\Delta\sigma = 1\ cm^{-1}$) | | | |
| Wavelength ($\mu$m) | 200 | 400 | 670 |
| Point source (mJy) | 120 | 125 | 250 |
| Map (mJy) | 310 | 335 | 670 |

## 7. The SPIRE consortium

SPIRE is being built by a consortium of European, American and Canadian scientists from the following groups: Caltech/Jet Propulsion Laboratory, Pasadena; Cardiff University, UK; CEA Service d'Astrophysique, Saclay, France; Institut d'Astrophysique Spatiale, Orsay, France; Imperial College, London, UK; Instituto de Astrofisica de Canarias,

Tenerife, Spain; Istituto di Fisica dello Spazio Interplanetario, Rome, Italy; Laboratoire d'Astronomie Spatiale, Marseille; Mullard Space Science Laboratory, Surrey, UK; NASA Goddard Space Flight Center, Maryland, USA; Observatoire de Paris, Meudon, Paris; Queen Mary and Westfield College, London, UK; UK Astronomy Technology Centre, Edinburgh, UK; Rutherford Appleton Laboratory, Oxfordshire, UK; Stockholm Observatory, Sweden; Università di Padova, Italy; University of Saskatchewan, Canada.


## Acknowledgements

Many people are participating in the design and manufacture of SPIRE. Those who have contributed to the technical definition addressed in this paper include: Peter Ade, Jean-Louis Augueres, Jean-Paul Baluteau, Rick Blaine, Jamie Bock, Terry Cafferty, Martin Caldwell, Christophe Cara, Riccardo Cerulli, Derek Coburn, John Coker, Patrick Collins, Dustin Crumb, Colin Cunningham, Pascal Dargent, John Delderfield, Kjetil Dohlen, Lionel Duband, Roger Emery, Didier Ferand, Martin Fisher, Alberto Franceschini, Walter Gear, Jason Glenn, Doug Griffin, Peter Hargrave, Peter Hamilton, Martin Harwit, Vic Haynes, Raul Hermoso, David Henry, Viktor Hristov, Don Jennings, Ken King, Andrew Lange, Jerry Lilienthal, Françoise Loubere, Bruno Maffei, Jerome Martignac, Guy Michel, Fraser Morrison, Harvey Moseley, Anthony Murphy, David Naylor, Hien Nguyen, Göran Olofsson, Seb Oliver, Renato Orfei, Ian Pain, Ismael Perez-Fournon, Frederic Pinsard, Dominique Pouliquen, Faiz Rahman, Tony Richards, Louis Rodriguez, Jaun Roman, Michael Rowan-Robinson, Paolo Saraceno, Srinivasan Sethuraman, Dave Smith, Chris Stell, Rashmi Sudiwala, Brian Stobie, Carole Tucker, Anthony Turner, Berend Winter, Adam Woodcraft, Gillian Wright.


## References


Ade, P.A.R., Hamilton, P.A., & Naylor, D.A., In *Fourier transform spectroscopy: new methods and applications*, OSA, 90, 1999.

Bock, J.J., Glenn, J., Grannan, S., Irwin, K.D., Lange, A.E., Leduc, H.G., & Turner, A.D., Proc. SPIE 3357, 297, 1998.

Caldwell, M.E., Swinyard, B.M., & Richards, A., Proc. SPIE 4013, 2000.

Dohlen, K, Origné a, A, Pouliquen, D, & Swinyard, B., Proc. SPIE 4013, 119, 2000.

Duband, L., Proc. of ESA Symposium on *The Far Infrared and Submillimetre Universe*, Grenoble, 15-17 April 1977, ESA SP-401, 357, 1997.

Eales, S., Lilly, S., Webb, T., Dunne, L., Gear, W., Clements, D., & Yun, M., Astron. J., 120, 2244, 2000.

Holland, W.S., Robson E.I., Gear W.K., Cunningham C.R., Lightfoot, J.F. Jenness, T., Ivison, R. J., Stevens, J.A., Ade, P.A.R, Griffin, M.J., Duncan, W.D., Murphy, J.A., & Naylor, D. A., Mon. Not. R. Astron. Soc. 303, 659, 1999.

Hughes, D.H., Serjeant, S., Dunlop, J., Rowan-Robinson, M., Blain, A., Mann, R., Ivison, R., Peacock, J., Efstathiou, A, Gear, W., Oliver, S., Lawrence, A., Longair, M., Goldschmidt, P., & Jeness, T. Nature 394, 241, 1998.

Mauskopf, P.D., Bock, J.J, del Castillo, H., Holzapfl, W. L, & Lange A. E., Appl. Opt. Vol. 36, No. 4, 765, 1997.

Pilbratt, G., Proc. of *The Promise of FIRST* symposium, 12-15 December 2000, Toledo, Spain, G.L Pilbratt, J. Cernicharo, A.M. Heras, T. Prusti & R. Harris eds., ESA SP-460 (this volume), 2001.

Smail, I, Ivison, R, Blain, A & Kneib, J.-P., Proc. 9th Annual October Astrophysics Conference, Maryland, 12-14 October, 1998, *After the Dark Ages: When Galaxies Were Young*, American Institute of Physics Press, p. 312, 1999.

Swinyard, B.M., Ade, P.A.R., Griffin, M.J., Hamilton, P.A., Dohlen, K., Baluteau, J.-P., Pouliquen, D., Ferand, D., Dargent, P., Michel, G., Martignac, J., Rodriguez, L., Jennings, D.E., Caldwell, M.E., & Richards, A.G., Proc. SPIE 4013, 196, 2000.